Impact of Catalyst Acid/Metal Balance in Hydroisomerization of Normal Paraffins

T. F. Degnan and C. R. Kennedy
Paulsboro Research Laboratory, Mobil Research and Development Corp. Paulsboro, NJ 08066

The hydroisomerization of n-heptane has been used as a model to study the acid-metal balance requirements for Pt/zeolite catalysts. Experiments were carried out using physical mixtures of zeolite beta and Pt/Al_2O_3 particles, in which the level of the metal-containing component was varied to change the acid-metal balance. Selectivity, in terms of cracking vs. isomerization, varies significantly with the metal loading up to a point beyond which the degree of paraffin isomerization is independent of metal loading. These results are interpreted in terms of a simple dual-site model based on a classical theory of polyfunctional catalysis, first advanced by Weisz (1962). The model is also used to show how an imbalance in hydrogenation and acid functions can even alter the apparent reaction network of the observable chemical species in the system.

Introduction

Bifunctional catalysts that comprise both acid and metal catalytic functions are used widely in the petroleum refining industry in such processes as light paraffin isomerization, naphtha reforming, and gas oil hydrocracking. A large body of literature exists on various aspects of these processes including the chemistry, catalysis, and commercial performance. Weisz (1962) proposed a general theory for polyfunctional catalysis and defined requirements on the balance between acid and metal activity in bifunctional catalysts to achieve the desired degree of hydrocarbon conversion. Coonradt and Garwood (1964) studied the mechanism of paraffin hydrocracking and the role of the hydrogenation component on dual-functional catalysts.

In the late 1960s, emphasis shifted away from amorphous acidic catalysts and toward the use of zeolites as the acidic component for many dual functional reactions. Zeolites offered a higher density of acid sites in a uniform pore structure. By the early 1970s, Shell commercialized a light paraffin, dual functional hydroisomerization process based on aluminum deficient mordenite catalyst that contained a noble metal (Kouwenhoven, 1971).

More recently, Steijins et al. (1981), Weitkamp (1982), Jacobs et al. (1982, 1986), and Martens et al. (1986a,b, 1991) have used the dual functional isomerization of straight chain paraffins to probe the effects of zeolite pore size and channel geometry on isomerization and hydrocracking reaction pathways. Octane, decane, and dodecane were reacted over noble metal-containing zeolites with different degrees of acidity to probe zeolite shape-selective constraints. Similar studies were carried out with *n*-hexane and Pt/zeolite beta (Leu et al., 1991).

In looking at the kinetics and reaction mechanisms of these dual functional catalysts, it is often assumed that catalysts are "ideal" in the sense that the metal component is present in sufficient excess to establish an equilibrium between saturated and associated unsaturated species. This simplifies matters greatly since in this case only the acid functionality needs be considered as rate-limiting. While this may be true for a well designed fresh catalyst, in actual usage the situation may change. The "acid/metal balance" of the catalyst may be shifted by selective poisoning or nonuniform deactivation of the individual components, a loss in metal surface area by mechanisms such as sintering or competitive adsorption in mixtures which can change the actual availability of individual sites.

In this article, we look at the impact of the acid/metal balance on isoparaffin selectivity during the hydroisomerization of normal paraffins. Experiments were carried out using a "separate particle" approach to vary the relative acid and

metal activities. The results not only give insights into the optimal design of catalysts but also suggest diagnostic approaches to evaluating the state of catalysts in actual commercial usage.

Experimental Studies

Five catalysts were prepared to evaluate the impact of varying metal loading on a catalyst with fixed acid activity. The separate particle approach was taken to control accurately the level of metals addition, while ensuring that catalyst preparation procedures did not affect the results. Physical mixtures of 1–40 μ particles of Pt/Al_2O_3 (1.15% Pt), zeolite beta ($SiO_2/Al_2O_3 = 135$), and inert γ-alumina were prepared as shown in Table 1. In this series of catalysts, the zeolite beta loading was kept constant and the γ-alumina was added as a filler. Zeolite beta was synthesized by a method similar to that described by Wadlinger et al. (1967).

The Pt dispersion (D_h = fraction exposed) of the Pt/Al_2O_3 catalyst was 0.68. MAS-NMR indicated that there was virtually no nonframework aluminum in the zeolite beta sample. Each zeolite beta + Pt/Al_2O_3 + Al_2O_3 mixture was pelleted, crushed, and sieved to 20–40 mesh prior to use.

In a typical run, 1 cm^3 of catalyst was charged to a packed tubular reactor with a preheat zone. The reactor and preheater were immersed in a fluidized-bed sand bath for isothermal temperature control. All catalyst samples were reduced in hydrogen at 350°C for 12 hours prior to streaming with *n*-heptane (Aldrich, Gold Label, 99.99%). Runs were conducted on each catalyst at 400 psig (2.8 MPa), 5.36 molar hydrogen/hydrocarbon ratio, and an LHSV of 20 h^{-1} based on zeolite. Conversion of the *n*-heptane charge was varied by changing reaction temperature. After each series of runs, one or more of the earlier sets of conditions was repeated as a check on catalyst activity and selectivity. There was no catalyst aging during these experiments.

The product analysis was performed on-line with a Varian 3700 gas chromatograph equipped with a 50-m fused silica WCOT OV-101 column (Supelco). The cracked products were primarily propane and butane. In these experiments, the C_7 products were predominantly mono-, di- and tribranched methyl paraffins. A small amount of ethyl pentane and methyl cyclohexane was formed (<2%), and these are included with the total isomer yields. When discussing individual isomers, they are lumped with the monomethyl hexanes. The percentage yield of a particular product fraction *i* is calculated as 100 $W_i/W_{n\text{-}C7}$, where W_i represents the weight of the product fraction *i*, and $W_{n\text{-}C7}$ represents the weight of the *n*-heptane fed. Conversion is defined as 1-$W_{n\text{-}C7}$ (product)/$W_{n\text{-}C7}$ (feed).

Results

Figure 1 shows *n*-heptane conversion and C_7-isomer yields vs. temperature for the five catalysts. Very little conversion was observed over the Pt-free catalyst in the temperature range shown here. Clearly, the addition of even small amounts of platinum significantly increases conversion activity. This effect is attributed to the generation of olefins via dehydrogenation over the noble metal and the subsequent role of these olefins in facilitating carbenium ion rearrangements (Weisz, 1962). We see that no additional conversion activity is observed above a loading of 0.54 m^2 Pt/g of zeolite for reaction temperatures

Table 1. Bifunctional Hydroisomerization Catalyst

Catalyst	Pt/Al_2O_3* (wt. %)	Zeolite** (wt. %)	γ-Al_2O_3+ (wt. %)	Pt Loading (wt. % of Total Cat.)	Pt Surface Area (m^2/g Zeolite)
0	-0-	50	50	0	0
1	2.6	50	47.7	0.03	0.084
2	5.6	50	44.4	0.064	0.180
3	16.7	50	33.3	0.192	0.540
4	50	50	-0-	0.575	1.61

*Pt/Al_2O_3 = 1.15% Pt, D_h = 0.68.
**SiO_2/Al_2O_3 = 135:1.
+Same Al_2O_3 as used in preparation of Pt/Al_2O_3.

greater than 375°C. Here, we have elected to express the required metal activity in terms of exposed Pt surface area. We assumed that Pt atoms have a diameter of 1.32 Å.

Figure 2a is a plot of isoheptane yield vs. *n*-heptane conversion for various Pt loadings. Here, the distinct maxima in the isomer yield vs. conversion vary as a function of Pt loading. Figure 2b plots the maximum isomer yield in wt.% vs. Pt loading. Two regions appear. Below approximately 0.6 m^2 Pt/g of zeolite, the isomer yield changes dramatically with Pt loading. Above 0.6 m^2 Pt/g of zeolite, the slope of the curve tends toward zero. Hence, this figure shows that the acid-metal balance for this Pt/Al_2O_3 zeolite sample is achieved at a Pt loading of 0.6 m^2 Pt/g of zeolite. This corresponds to one exposed Pt atom for every six framework aluminum atoms in the zeolite beta sample.

Kinetic Analysis

Consider a general reaction network which groups structural isomers by the number of methyl branches on a molecular chain. Following the classical bifunctional route proposed by Weisz (1962) and Coonradt and Garwood (1964), isomerization plus cracking can be represented by the following scheme 1:

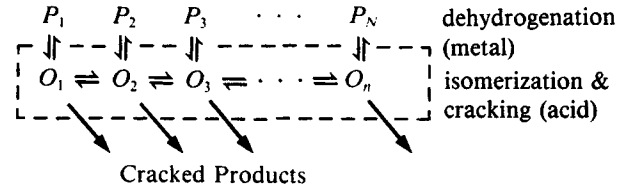

where
P_i = paraffins of a fixed carbon number containing *i* branches
O_i = olefins of a fixed carbon number containing *i* branches

The dehydrogenation/hydrogenation on the metal site acts as the initiation/termination step in the formation of olefinic reaction intermediates. The actual isomerization and cracking take place through these olefinic intermediates on the acidic catalyst sites through classical carbenium ion chemistry (Martens and Jacobs, 1990).

The continuity equations in a plug-flow reactor can be written as:

$$\frac{d\underline{F}_p}{dx} = -W_{cat}\underline{R}_m$$

$$\frac{d\underline{F}_o}{dx} = W_{cat}[\underline{R}_m - \underline{R}_a] \quad (1)$$

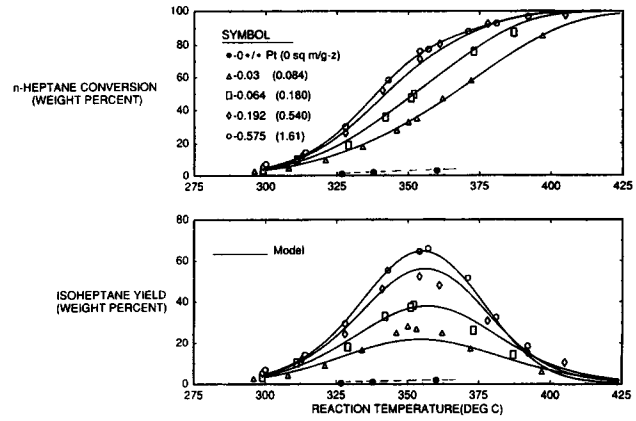

Figure 1. Isomerization selectivity: *n*-heptane conversion and isoheptane yields vs. temperature.

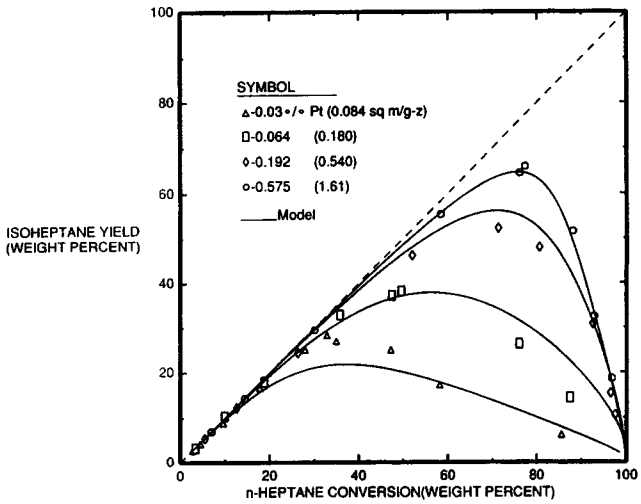

Figure 2a. Isoheptane yield vs. *n*-heptane conversion: model vs. observed.

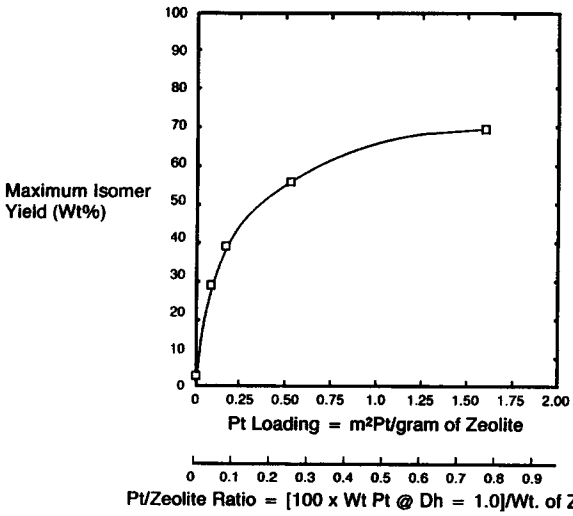

Figure 2b. Maximum isoheptane yield vs. Pt/zeolite ratio.

Pt loading normalized for % Pt exposed.

where $\underline{F}_p$ and $\underline{F}_o$ are vectors of molar flow rates (mol/s) and $\underline{Rm}$ and $\underline{Ra}$ are vectors of reaction rates (mol/g cat/s) on the metal and acid sites, respectively. Wcat is the catalyst loading (g), and x is a dimensionless reactor length.

Dehydrogenation

Following Dumez and Froment (1976), we assume a mechanism for paraffin dehydrogenation, which can be represented by the following steps:

$$\begin{array}{ll} P+m \rightleftharpoons P^* & K_1 = C_p/mP_p \\ P^*+m \rightleftharpoons O^*+H_2^* & K_2 = C_oC_H/mC_P \\ O^* \rightleftharpoons O+m & K_3 = mP_o/C_o \\ H_2^* \rightleftharpoons H_2+m & K_4 = mP_H/C_H \\ \hline P \rightleftharpoons O+H_2 & \end{array}$$

where P's represent partial pressures, C's are surface concentrations, and m is the concentration of metal sites. The superscript $(\,)^*$ represents adsorbed species. Assuming that dissociation is the rate-limiting step:

$$R_m = \hat{k}_d\langle m\rangle C_p - \hat{k}_h\langle H_2\rangle C_o \tag{2}$$

Here, $\langle\cdot\rangle$ represents a probability, in which the adjacent site has the required occupancy (see Froment and Bischoff, 1979, p. 98). In terms of fractional coverages, θ:

$$m = m_T\theta_v \quad C_H = m_T\theta_H \quad C_p = m_T\theta_p \quad C_o = m_T\theta_o$$

$$\langle m\rangle = \frac{sm_T\theta_v}{m_T} = s\theta_v \quad \langle H_2\rangle = \frac{sm_T\theta_H}{m_T} = s\theta_H$$

where s is the number of nearest neighbor sites, and m_T is the total number of metal sites/g of catalyst. Then,

$$R_m = m_T\theta_v^2\left[(s\hat{k}_dK_1)P_P - \left(\frac{s\hat{k}_h}{K_3K_4}\right)P_HP_o\right] \tag{3}$$

or in vector notation along the lines developed by Wei and Prater (1962):

$$\underline{R}_m = m_T\theta_v^2(\underline{K}_d\underline{P}_p - P_H\underline{K}_h\underline{P}_o) \tag{4}$$

where $k_d = s\hat{k}_dK_1$, and $k_h = s\hat{k}_h/K_3K_4$ are the elements of the diagonal matrices $\underline{K}_d$ and $\underline{K}_h$. At equilibrium:

$$P_H^e\underline{P}_o^e = \underline{K}_h^{-1}\underline{K}_d\underline{P}_p^e \equiv \underline{K}_{eq}\underline{P}_p^e \tag{5}$$

and we can write Eq. 4 in terms of the equilibrium constant for dehydrogenation:

$$\underline{R}_m = m_T\theta_v^2\underline{K}_d(\underline{P}_p - P_H\underline{K}_{eq}^{-1}\underline{P}_o) \tag{6}$$

Isomerization and Cracking

On the acid sites, olefinic intermediates follow a sequence of adsorption, rearrangement or cracking and desorption. The following reaction scheme shows this for an olefinic intermediate O_j:

$$O_j + a \rightleftharpoons O_j^+ \qquad K_S^{(j)} = C_o^{(j)}/aP_o^{(j)}$$
$$O_{j-1}^+ \rightleftharpoons O_j^+ \rightleftharpoons O_{j+1}^+$$
$$O_j^+ \rightarrow \text{cracked products} + a$$

Here, $(\,)^+$ represents surface carbenium ions. Assuming isomerization and cracking are the slow steps and taking $a = a_T\psi_v$, where a_T is the total number of acid sites/g of catalyst and ψ_v is the fractional vacancy:

$$\underline{R}_a = a_T\psi_v(\underline{\underline{\hat{K}}}_i + \underline{\underline{\hat{K}}}_c)\underline{P}_o \tag{7}$$

$\underline{\underline{\hat{K}}}_c$ is the diagonal cracking rate constant matrix with elements $\{k_c^{(j)}K_S^{(j)}\}$, and $\underline{\underline{\hat{K}}}_i$ is the tridiagonal isomerization matrix with elements:

$$(-k_i^{(j-1)}K_S^{(j-1)}),\ (\bar{k}_i^{(j-1)} + k_i^{(j)})K_S^{(j)},\ (-\bar{k}_i^{(j)}K_S^{(j+1)})$$

along the tridiagonal band. Here, the overbar denotes the reverse rate constant. For future convenience, let:

$$\underline{\underline{K}}_i \equiv \underline{\underline{\hat{K}}}_i\underline{\underline{K}}_{eq} \qquad \underline{\underline{K}}_c \equiv \underline{\underline{\hat{K}}}_c\underline{\underline{K}}_{eq}$$

then,

$$\underline{R}_a = a_T\psi_v(\underline{\underline{K}}_i + \underline{\underline{K}}_c)\underline{\underline{K}}_{eq}^{-1}\underline{P}_o \tag{8}$$

With these rate expressions, the continuity equations (Eqs. 1) become:

$$\frac{d\,\underline{F}_p}{dx} = -W_{cat}m_T\theta_v^2\underline{\underline{K}}_d(\underline{P}_p - P_H\underline{\underline{K}}_{eq}^{-1}\underline{P}_o)$$

$$\frac{d\,\underline{F}_o}{dx} = W_{cat}[m_T\theta_v^2\underline{\underline{K}}_d(\underline{P}_p - P_H\underline{\underline{K}}_{eq}^{-1}\underline{P}_o) - a_T\psi_v(\underline{\underline{K}}_i + \underline{\underline{K}}_c)\underline{\underline{K}}_{eq}^{-1}\underline{P}_o] \tag{9}$$

Stationary State Hypothesis

Olefin concentrations are generally small along with the magnitude of their concentration changes (Weisz, 1962). Then,

$$0 = m_T\theta_v^2\underline{\underline{K}}_d(\underline{P}_p - P_H\underline{\underline{K}}_{eq}^{-1}\underline{P}_o) - a_T\psi_v(\underline{\underline{K}}_i + \underline{\underline{K}}_d)\underline{\underline{K}}_{eq}^{-1}\underline{P}_o \tag{10}$$

which can be rewritten to give:

$$\underline{P}_p = \left[\underline{\underline{I}} + \frac{\sigma}{P_H}\underline{\underline{K}}_d^{-1}(\underline{\underline{K}}_i + \underline{\underline{K}}_c)\right]\underline{\underline{K}}_{eq}^{-1}\underline{P}_oP_H \tag{11}$$

where $\sigma = a_T\psi_v/m_T\theta_v^2$ represents the acid/metal balance of the catalyst. The acid/metal balance technically depends on the individual rate constant ratios through all the terms added to the identity matrix in Eq. 11, but since metal site turnover rates are generally larger than acid site rates, $\|\underline{\underline{K}}_d^{-1}(\underline{\underline{K}}_i + \underline{\underline{K}}_c)\|$ is small and the parameter σ/P_H controls the deviation of Eq. 11 from the equilibrium relationship (Eq. 5).

Excess Metal

If σ/P_H is sufficiently small, Eq. 11 reduces to Eq. 5:

$$\underline{P}_p = \underline{\underline{K}}\text{eq}^{-1}\underline{P}_oP_H \tag{12}$$

which says olefins are present in pseudo-equilibrium with the local paraffin concentrations. Then,

$$\frac{d\,\underline{F}_p}{dx} = -W\text{cat}\,\frac{a_T\psi_v}{P_H}(\underline{\underline{K}}_i + \underline{\underline{K}}_c)\underline{P}_p \tag{13}$$

This is generally the form assumed in evaluating kinetics of paraffin hydrocracking (Baltanas et al., 1983).

Metals Not in Excess

The parameter σ/P_H can be nonnegligible for a number of reasons. The catalyst can be poorly designed (m_T small), or metal surface area can be lost through sintering (D_h small). Also, hydrogen partial pressure can be too low, or metal sites can be lost through poisoning, deactivation, or competitive adsorption (θ_v small). It should be noted that the effective acid/metal balance depends on the actual reactor environment, not just the catalyst synthesis variable (a_T/m_T). In this case,

$$\frac{d\,\underline{F}_p}{dx} = -W\text{cat}\,\frac{a_T\psi_v}{P_H}(\underline{\underline{K}}_i + \underline{\underline{K}}_c) \times \left[\underline{\underline{I}} + \frac{\sigma}{P_H}\underline{\underline{K}}_d^{-1}(\underline{\underline{K}}_i + \underline{\underline{K}}_c)\right]^{-1}\underline{P}_p \tag{14}$$

It is clear that Eq. 13 is just a special case of Eq. 14 as σ approaches zero.

Lack of metal function alters the selectivity of the process through the term $[\underline{\underline{I}} + (\sigma/P_H)\underline{\underline{K}}_d^{-1}(\underline{\underline{K}}_i + \underline{\underline{K}}_c)]^{-1}$. When metal is present in sufficient excess, the olefin intermediate concentration for any isomer is related only to the concentration of the corresponding (observable) paraffin isomer. In case metal activity is not sufficient to ensure validity of an equilibrium assumption, the situation is considerably more complex. The concentration of olefinic intermediates depends on the concentration of *all* the paraffin isomers present through Eq. 11. In this case, the surface reactions tend to "scramble" the apparent chemistry. An olefinic intermediate may enter the "black box" in scheme 1, which contains the (unobservable) reaction intermediates on the acid sites and undergo several reactions before hydrogenation back to an observable gas-phase species. Under these conditions, the apparent reaction network of the observable species can actually change.

This can be more clearly seen by way of a simple example.

Simple Example

Consider the case where species are lumped as normal paraffins, isoparaffins, and cracked products. Furthermore, consider isomerization as irreversible. (This case is considered for mathematical simplicity. The reversible case can be worked out but it is a bit more tedious.) If we follow the conventional assumption (Martens and Jacobs, 1990) that normal olefins do not crack, then the reaction scheme can be written as the following scheme 2:

$$\begin{array}{ccccc} P_n & & P_i & & \\ \Downarrow\Uparrow & & \Downarrow\Uparrow & & \\ O_n & \xrightarrow[k_i]{} & O_i & \xrightarrow[kc]{} & \text{cracked products} \end{array}$$

In Eq. 14,

$$\underline{\underline{K}}_i = \begin{bmatrix} k_i & 0 \\ -k_i & 0 \end{bmatrix} \quad \underline{\underline{K}}_c = \begin{bmatrix} 0 & 0 \\ 0 & k_c \end{bmatrix} \quad \underline{\underline{K}}_d = \begin{bmatrix} k_{dn} & 0 \\ 0 & k_{di} \end{bmatrix}$$

The continuity equations for normal and isoparaffins become:

$$\frac{d}{dx}\underline{F}_n = -\phi k_i^e P_n$$

$$\frac{d}{dx}\underline{F}_i = \phi[\nu k_i^e P_n - k_c^e P_i] \tag{15}$$

where

$$\phi = W\text{cat}\,\frac{a_T \psi_v}{P_H} \qquad \nu = \frac{1}{1+\sigma k_c/P_H k_{di}}$$

$$k_i^e = \frac{k_i}{1+\sigma k_i/P_H k_{dn}} \qquad k_c^e = \frac{k_c}{1+\sigma k_c/P_H k_{di}}$$

Thus, the *effective* rate constant for disappearance of the normal paraffin increases with increasing metals content, and k_i^e will approach k_i as a limit asymptotically, consistent with the data in Figure 1. It also says that overall rate will be inhibited by higher hydrogen pressures through reduction of the intermediate olefin concentration, which is also well known.

In terms of a selectivity equation, we can write:

$$\frac{dY_i}{dY_n} = -\nu + \lambda \frac{Y_i}{Y_n}$$

where

$\lambda = k_c^e/k_i^e$

Y = moles of respective component per mole of feed

In general this equation is nonlinear, since σ depends on composition through the competitive adsorption terms. However, if σ is considered a constant, then the yield of isoparaffins is given by:

$$Y = \frac{\nu}{1-\lambda}\left[(1-X)^{\lambda} - (1-X)\right]$$

when the charge is pure normal paraffin. Here, Y is the isoparaffin yield, and X is the normal paraffin conversion. This is shown in Figure 3a for constant λ and variable ν. The maximum in the curve is given by:

$$Y_{\max} = \nu\lambda^{\lambda/1-\lambda}$$

The impact of low metal activity is seen as follows. When metal activity is high, $\nu \sim 1$ and the apparent kinetic scheme (in terms of the observables) is the consecutive reaction sequence, as shown in the following scheme 3:

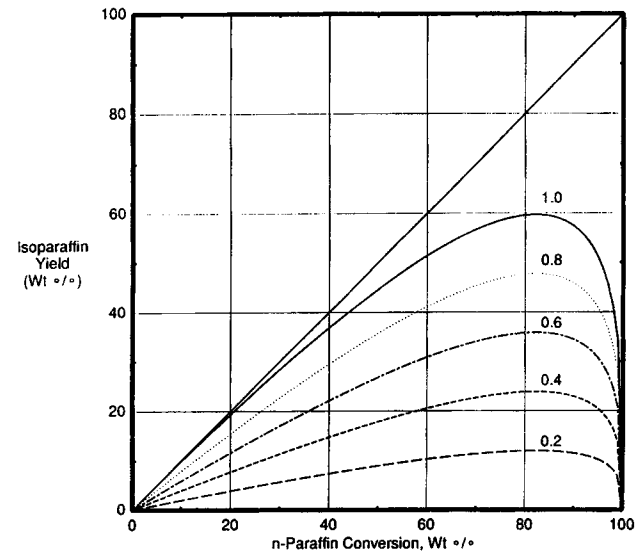

Figure 3a. Impact of acid/metal balance ($1/\sigma$) on isoparaffin selectivity.

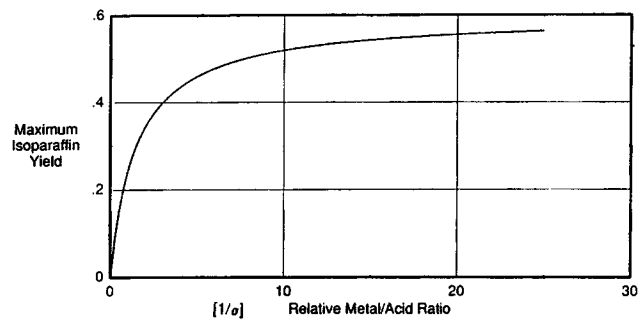

Figure 3b. Impact of acid/metal balance on maximum isoparaffin yield.

$$P_n \rightarrow P_i \rightarrow \text{Cracked Products}$$

But with low metal function, $\nu < 1$, the effective scheme (scheme 4) is:

$$\begin{array}{l} \overset{1-\nu}{\rightarrow} \\ P_n \rightarrow P_i \rightarrow \text{Cracked Products} \\ \underset{\nu}{\rightarrow} \end{array}$$

That is, it appears as though normal paraffins are cracking directly to lighter products with selectivity $1-\nu$. Although the linear olefins do not crack directly, they may undergo several steps as intermediates before being converted back to the observable components.

The term λ can be expected to be relatively insensitive to acid/metal balance, since there are compensating terms with the same functional dependence on σ in both the numerator and denominator:

$$\lambda = \frac{k_c}{k_i}\,\frac{1+\sigma k_i/P_H k_{dn}}{1+\sigma k_c/P_H k_{di}}$$

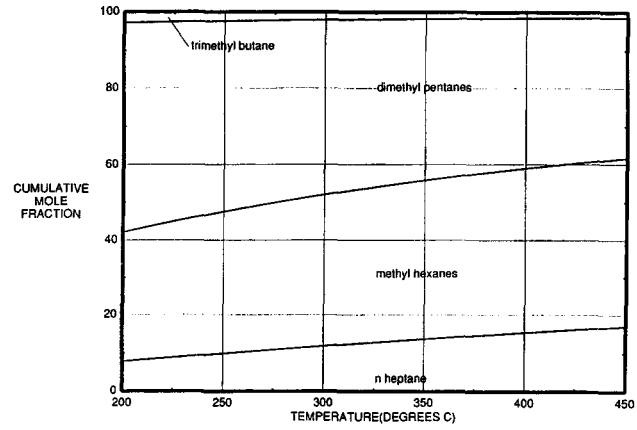

Figure 4a. Effect of temperature on heptane isomer equilibrium distribution.

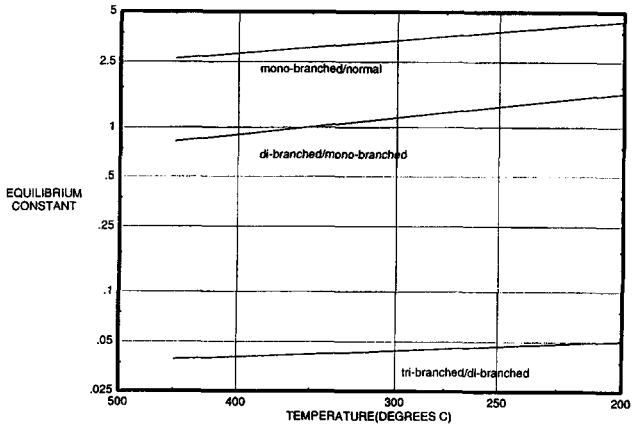

Figure 4b. Heptane isomer equilibrium constants.

Conversely ν depends strongly on the value of σ. Figure 3a shows the selectivity curves parameterized by the variable ν, while Figure 3b shows the maximum yield increasing to its asymptotic limit with increasing metal activity $[1/\sigma]$. These figures clearly capture many of the qualitative features of the data in Figures 2a and 2b.

While this simple example explains some of the features, there are important differences as well. The main feature is that in the simple model, the initial slope of the selectivity curve in Figure 3a is ν, which decreases with lower metal activity. The actual data in Figure 2a shows that the initial slope of the yield curve is unity, regardless of metal loading.

Lumping By Degree of Branching

Grouping all isomers together as one kinetic lump is too coarse an approximation to capture the details of the actual kinetics. It has been seen quite clearly (Baltanas et al., 1983; Dumez and Froment, 1976; Froment and Bischoff, 1979; Martens et al., 1991) that neither the normal nor monobranched isomers crack and that multiple branching is required. To this end, we consider a model consisting of four observable paraffin lumps (0 to three branches) plus cracked products and evaluate rate constants from the kinetic data. To reduce the number of parameters involved, the reversible isomerization reactions were

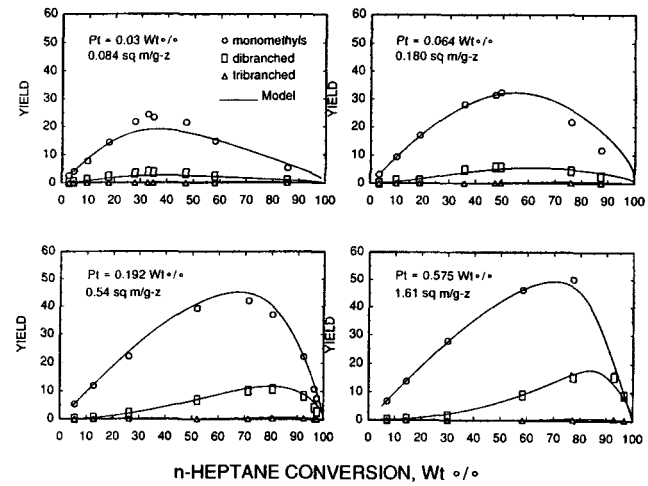

Figure 5. Heptane isomer distributions vs. *n*-heptane conversion for different Pt/zeolite ratios.

expressed in terms of equilibrium constants for paraffin isomerization. The effect of temperature on the equilibrium distribution of heptanes is shown in Figures 4a and 4b. These plots were calculated from data given by Stull et al. (1969). Figure 4a shows that as temperature increases, equilibrium favors less highly branched isomers.

Reversible rates in the isomerization scheme can be expressed in terms of the equilibrium constant for the reaction $K_i^{(j)}$:

$$\overline{k}_i^{(j)} = k_i / K_i^{(j)} \qquad \text{where} \quad K_i^{(j)} = P_{j+1}^e / P_j^e$$

$$K_i^{(j)} = K_i^{o(j)} e^{(-\Delta G/RT)}$$

Using the data from Stull et al. (1969), we estimate:

Equilibrium	K_i^o	ΔG
mono/normal	0.989	−1,400
di/mono	0.236	−1,800
tri/di	0.024	−700

Figure 4b shows the relative values of K_i as a function of temperature on an Arrhenius plot.

The results of lumping the reaction mechanism by degree of branching are shown in Figure 5. Here, the theoretical isomer yields, lumped by degree of branching, are compared with the empirical data as a function of *n*-heptane conversion. As conversion increases, the monomethyl isomer concentration passes through a maximum at a lower conversion than the dibranched isomer concentration. Few tribranced isomers are formed. The acid-metal balance has a profound effect on the position of the yield maxima. The maxima move to higher *n*-heptane conversions as the metal function increases relative to the acid function.

Figure 6 shows the same results as a function of temperature. The temperatures at which the yield maxima occur for the mono- and dibranched isomers do not change with the amount of Pt on the catalyst.

In this analysis, only the forward rates (preexponential factor and activation energy) were adjusted to match the data. Reverse

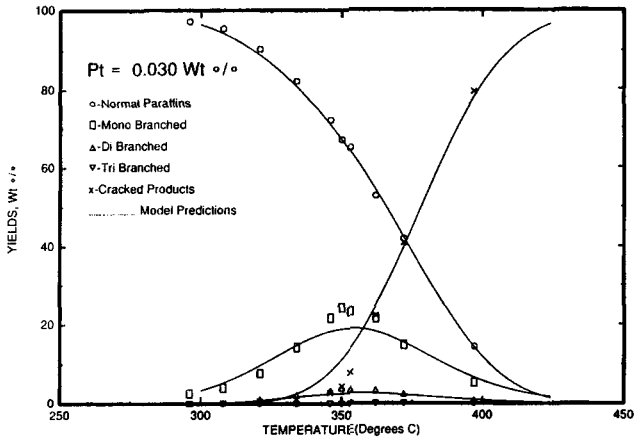

Figure 6a. Heptane product distribution vs. reaction temperature for Pt = 0.03 wt. % case.

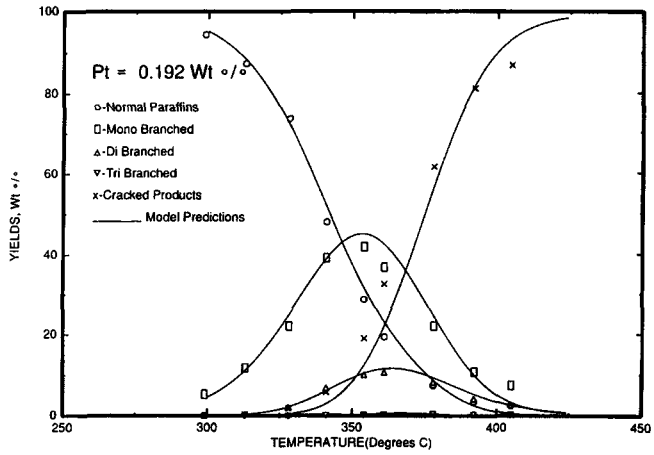

Figure 6c. Heptane product distribution vs. reaction temperature for Pt = 0.192 wt. % case.

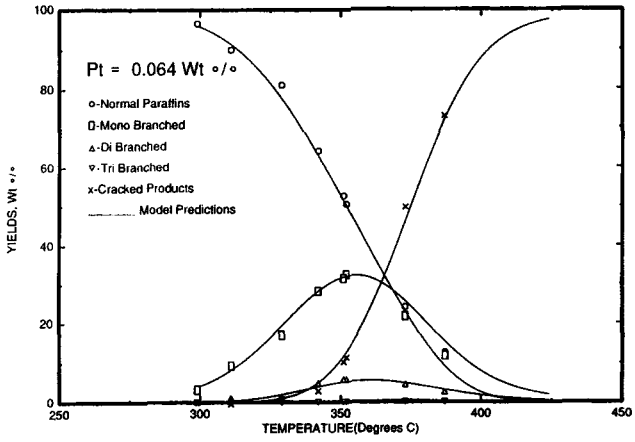

Figure 6b. Heptane product distribution vs. reaction temperature for Pt = 0.064 wt. % case.

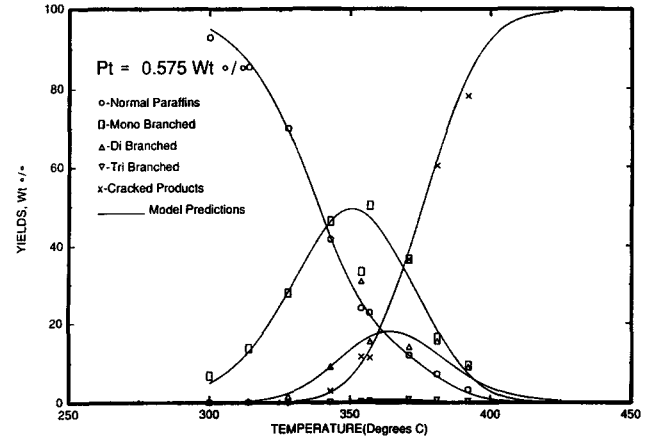

Figure 6d. Heptane product distribution vs. reaction temperature for Pt = 0.575 wt. % case.

rates were determined using the estimated values of the equilibrium constants. This model still neglects the effects of competitive adsorption.

Total isomer yields are shown as the solid lines in Figures 2a and 1b and normal paraffin conversion is shown in Figure 1a. This model captures most of the data trends as seen in Figure 5. The remainder of the deviations from the data come about because of nonlinear interaction brought on by the concentration effects on θ_v and ψ_v, here assumed constant. We will analyze these effects in more detail in the future.

Conclusions

The balance between acid and metal activities on bifunctional catalysts can have dramatic effects on the selectivity of desired products in a reacting system. The effect can even change the apparent reaction networks of the observable kinetic components. Here, we have used hydroisomerization of normal heptane to show these effects and have interpreted the data both qualtitatively and quantitatively through kinetic models based on Weisz's general theory of polyfunctional catalysis. These effects can be expected to be present in other bifunctional systems such as reforming where the addition of ring closure and hydrogenolysis will make the selectivity picture even more complex. Recent work by Beltramini et al. (1991) has shown the utility of using a dual-site approach in studying deactivation of reforming catalysts.

Notation

a = concentration of acid sites, mols/g cat
C = surface concentration, mols/m^2
D_h = fractional dispersion of the metal = fraction exposed
F_o = molar flow rate of olefin, mol/s
F_p = molar flow rate of paraffin, mol/s
I = identity matrix
k = rate constant, s^{-1}
K = equilibrium constant
$\underline{\underline{K}}_c$ = cracking rate constant matrix
$\underline{\underline{K}}_{eq}$ = equilibrium constant matrix
$\underline{\underline{K}}_i$ = isomerization rate constant matrix
m = concentration of metal sites, mol/g cat
O_i = olefin with i branches
P = partial pressure, torr
P_i = paraffin with i branches
R_a = reaction rate on the acid sites, mol/g cat/s
R_m = reaction rate on the metal sites, mol/g cat/s
s = number of nearest neighbor sites
T = temperature, K

W_{cat} = weight of catalyst, g
W_i = weight of product fraction i
$W_{n\text{-}C7}$ = weight of n-heptane
x = dimensionless reactor length
Y_i = moles of product component i per mole of feed

Greek letters

θ_v = fractional coverage (metal)
ψ_v = fractional vacancy (acid)
σ = acid-metal balance parameter $[= a_T\psi_v/m_T\theta^2{}_v]$
ν = dimensionless parameter def. in Eq. 15 $= 1/(1 + \sigma k_c/P_H k_{di})$
ϕ = dimensionless parameter def. in Eq. 15 $= W_{cat}(a_T\psi_v/P_H)$
λ = ratio of cracking to isomerization rate constants
ΔG = free energy of formation, kcal/mol K

Superscripts

* = adsorbed species
$^+$ = surface carbenium ions
^{e} = effective (as in effective rate constant)

Subscripts

d = dehydrogenation
dn = dehydrogenation of normal paraffins
di = dehydrogenation of isoparaffins
h = hydrogenation
H = hydrogen
i = isoparaffins
n = normal paraffins
o = olefin
p = paraffin
T = total number of sites
v = vacancies

Other

$\langle\ \rangle$ = probability that an adjacent site has an occupancy

Literature Cited

Baltanas, M. A., H. Vansina, and G. F. Froment, "Hydroisomerization and Hydrocracking 5. Kinetic Analysis of Rate Data for n-Octane," *Ind. Eng. Chem., Prod. Res. Dev.*, **22**, 531 (1983).

Beltramini, J. N., T. J. Wessel, and R. Datta, "Kinetics of the Deactivation of Bifunctional Pt/Al_2O_3-Cl Catalyst by Coking," *AIChE J.*, **37**, 845 (1991).

Coonradt, H. L., and W. E. Garwood, "Mechanism of Hydrcracking-Reactions of Paraffins and Olefins," *Ind. Eng. Chem., Process Des. Dev.*, **3**, 38 (1964).

Dumez, F. J., and G. F. Froment, "Dehydrogenation of 1-Butene into Butadiene Kinetics, Catalyst Coking and Reactor Design," *Ind. Eng. Chem., Process Des. Dev.*, **15**, 291 (1976).

Froment, G. F., and K. B. Bischoff, *Chemical Reactor Design and Analysis*, p. 98, Wiley, New York (1979).

Jacobs, P. A., and J. A. Martens, "The Potential and Limitations of the n-Decane Hydroconversion as a Test Reaction for the Characterization of Molecular Sieve Zeolites," *Zeolites*, **6**, 341 (1986).

Jacobs, P. A., J. A. Martens, J. Weitkamp, and H. K. Beyer, "Shape-Selectivity Changes in High-Silica Zeolites," *Farad. Discuss. Chem. Soc.*, **72**, 353 (1982).

Kouwenhoven, H. W., and W. C. VanZijll, "Shell's Hydro-Isomerization Process," *Chem. Eng. Prog.*, **67**, 65 (1971).

Leu, L.-J., L.-Y. Hou, B.-C. Kang, C. Li, S.-T. Wu, and J.-C. Wu, "Synthesis of Zeolite β and Catalytic Isomerization of n-Hexane over Pt/H-β Catalysts," *Appl. Catal.*, **69**, 49 (1991).

Martens, J. A., P. A. Jacobs, and J. Weitkamp, "Attempts to Rationalize the Distribution of Hydrocracked Products: I. Qualitative Description of the Primary Hydrocracking Modes of Long Chain Paraffins in Open Zeolites," *Appl. Catal.*, **20**, 239 (1986).

Martens, J. A., P. A. Jacobs, and J. Weitkamp, "Attempt to Rationalize the Distribution of Hydrocracked Products: II. Relative Rates of Primary Hydrocracking Modes of Long Chain Paraffins in Open Zeolites," *Appl. Catal.*, **20**, 283 (1986).

Martens, J. A., and P. A. Jacobs, "Conceptual Background for the Conversion of Hydrocarbons on Heterogeneous Acid Catalysts," *Theoretical Aspects of Heterogeneous Catalysis*, p. 52, J. B. Moffet, ed., Van Norstand Reinhold, New York (1990).

Martens, J. A., R. Parton, L. Uytterhoeven, P. A. Jacobs, and G. F. Froment, "Selective Conversion of Decane into Branched Isomers: A Comparison of Platinum/ZSM-22, Platinum/ZSM-5, and Platinum/USY Zeolite Catalysts," *Appl. Catal.*, **76**, 95 (1991).

Steijins, M., G. F. Froment, P. A. Jacobs, J. B. Uytterhoeven, and J. Weitkamp, "Hydroisomerization and Hydrocracking: 2. Product Distributions from n-Decane and n-Dodecane," *Ind. Eng. Chem. Prod. Res. Dev.*, **20**, 654 (1981).

Stull, D. R., E. F. Westrum, Jr., and G. G. Sinke, *The Chemical Thermodynamics of Organic Compounds*, Wiley, New York (1969).

Wadlinger, R. L., G. T. Kerr, and E. Rosinski, U.S. Patent 3,308,069 (1967), Reissued as U.S. Patent Re. 28,341 (1975).

Wei, J., and C. D. Prater, "The Structure and Analysis of Complex Reaction Systems," *Adv. in Catal.*, **13**, 203 (1962).

Weitkamp, J., "Isomerization of Long Chain n-Alkanes on a Pt/CaY Zeolite Catalyst," *Ind. Eng. Chem. Prod. Res. Dev.*, **21**, 550 (1982).

Weisz, P. B., "Polyfunctional Heterogeneous Catalysis," *Adv. in Catal.*, **13**, 137 (1962).

Manuscript received June 2, 1992, and revision received Sept. 18, 1992.